

NUMERICAL STUDY OF WIND-TUNNEL ACOUSTIC RESONANCE INDUCED BY TWO-DIMENSIONAL AIRFOIL FLOW AT LOW REYNOLDS NUMBER

**Tomoaki Ikeda^{*}, Takashi Atobe^{*}
Yasufumi Konishi^{**}, Hiroki Nagai^{**} and Keisuke Asai^{**}**
^{*}Japan Aerospace Exploration Agency, ^{}Tohoku University**

Keywords: *aeroacoustics, low Reynolds number flow, aerodynamic characteristics*

Abstract

In the aeroacoustic measurements of a wind-tunnel test, the acoustic resonance should be avoided, associated with the walled test section. The present numerical study of an NACA0012 airfoil focuses on how the wall resonance affects unsteady flow motions via a feedback process, by comparing with the airfoil placed in a free stream. Tonal frequencies observed in the present simulations agree well with our previous wind-tunnel experiments, represented approximately by the discrete resonant modes derived through a simple geometrical relation. More importantly, however, the present results indicate that rather strong wall resonance may alter the hydrodynamic flow measurements as well. The acoustic feedback process stimulates the transitional boundary layer on the suction side, which would increase lift force in the acoustically resonant channel by suppressing trailing-edge separation. At a higher angle of attack, the increment of lift force becomes more significant due to the noticeable size reduction of a separation bubble, understood via the comparison of three-dimensional instantaneous vortical structures.

1 Introduction

This paper presents the numerical simulations of a two-dimensional flow around an NACA0012 airfoil, confined within wind-tunnel walls at a low Reynolds number. Trailing-edge noise is often observed at moderate Reynolds number, as

acoustic scattering from a sharp edge when coherent eddies are shed into wake. The tonal noise emission is supposedly retained via the formation of an acoustic feedback loop, the resonance between hydrodynamic instability waves in boundary layer and acoustic disturbances traveling upstream. Specifically, at low Reynolds number, the frequency of tonal noise, or vortex shedding goes down to $O(1)$, normalized with chord length and uniform-flow velocity. In terms of unsteady aerodynamics, the emitted acoustic disturbance serves as an unsteady component of aerodynamic force. As shedding frequency lowers, the unsteady aerodynamic force may become non-negligible [3, 4].

In the experiments to measure airfoil tones, open jet facilities are often employed with anechoic environments [e.g., 2, 11]. In closed wind-tunnel environments, however, solid walls should be acoustically lined to avoid unwanted resonance within a test section [e.g., 7, 13]. Otherwise, a closed channel induces tones of acoustic resonance, whose frequency is determined mostly by the section height at low Mach number, less influenced by flow velocity [7, 10, 12]. Our previous experiment of an NACA0012 airfoil, conducted in the Mars Wind Tunnel [8] also shows fixed tones, nearly independent of flow velocity. The fixed tonal noise did not vanish completely even after an acoustic absorber was installed on the test section. In the study, one of the primary purposes was to attain experimental evidence of an acoustic feedback loop at low

Reynolds number, which turned out to be difficult under the influence of wall resonance.

The present paper discusses how the wall resonance affects the mechanism of airfoil tone generation. For this purpose, numerical simulations of two-dimensional NACA0012 airfoil are conducted with a rigid-wall boundary condition applied on the test-section walls. Under the influence of wall resonance, unsteady motions are altered from those observed in a uniform flow without external walls. We focus on how the acoustic disturbance due to wall resonance is fed back into the airfoil unsteadiness. In addition, it is of interest how the acoustic disturbance, amplified by the resonance in a wind tunnel, may alter the hydrodynamic state of an airfoil flow. The development of vortical motions in a suction-side boundary layer, prompted by an acoustic feedback loop, has a great effect on the formation of a laminar separation bubble [5]. The presence of a separation bubble at the leading edge can significantly improve the aerodynamic performance of an airfoil. The time-averaged flow field is compared with the case solved in a uniform flow.

2 Reference Experiment

We briefly summarize our previous experimental work [8] for the comparison with the present numerical study. The unsteadiness of low Reynolds number flows around an NACA0012 airfoil was examined in the Mars Wind Tunnel (MWT), the decompression experimental rig operated in a vacuum chamber. A wind-tunnel test can be conducted at reduced pressure, so that relatively high Mach number flows, up to approximately $M \sim 0.8$, can be achieved at low Reynolds number, in a range between 10^3 and 10^5 [1]. Geometrically two-dimensional test models can be placed in a walled test section. The spanwise width is 100 [mm], while the height is slightly diverged toward downstream to relax the effect of boundary-layer development on the channel walls. The mean height of the test section is 160 [mm].

In the experiment [8], high-frequency pressure transducers were mounted on both sides of the NACA0012 airfoil at 90% chord, with 50 [mm] chord length, to measure the pressure fluctuations associated with vortex shedding.

On the other hand, time-averaged pressure distributions were obtained by using the pressure-sensitive paint on the airfoil. The wind-tunnel tests were operated at chord-based Reynolds numbers $Re = 1.1 \times 10^4$ and 4.7×10^4 , at $M = 0.2$. In addition, Mach number dependence was further investigated as a follow-up study, by increasing Mach number up to $M = 0.4$. We will reference the experimental case at $Re = 1.1 \times 10^4$ to compare with the present numerical results.

3 Numerical Approach

Compressible Navier-Stokes equations are solved on multi-block structured numerical grid. Employed numerical schemes are summarized in our previous study [4]. Two-dimensional geometrical configurations are determined to mimic the MWT experiment [8]. An NACA0012 airfoil, with chord length L , is placed in the middle of a two-dimensional channel. The test-section height H is given as $3.2L$. We define x and y axes in the streamwise and wall normal directions, respectively. In three dimensional cases, z axis will be added in the spanwise direction with periodic boundary condition. The origin of the 2D x - y coordinates is defined at the trailing edge of the airfoil of chord length L . However, regardless of angle of attack α , the mid-chord location is fixed at the half height of the test section. In addition, the local X - Y coordinates are introduced in the chordwise and normal directions. Their origin comes to the leading edge of the airfoil.

The numerical domain is defined in the range of $-10 \leq x/L \leq 15$, while the test section of the actual wind tunnel corresponds to the region $-4.5 \leq x/L \leq 3.5$. In the experimental setup, a contraction region is introduced in the upstream section, while a diffuser section is added downstream with ejectors. In the present numerical study, characteristic inflow/outflow conditions are applied at both ends of the domain, with sponge layers to damp unwanted acoustic reflections. Inflow density and velocity are defined as ρ_∞ and U_∞ , and employed for non-dimensionalization, as well as characteris-

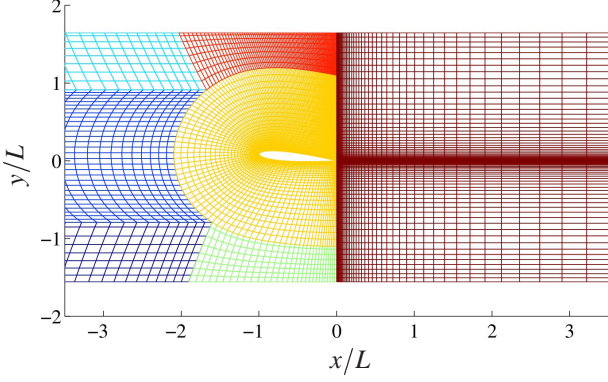


Fig. 1 Subset of numerical grid for an NACA0012 airfoil at the angle of attack $\alpha = 5^\circ$, settled in a wind tunnel. Each color indicates a block of structured grid, coarsened to the factor of four for visualization clarity.

tic length L . A free-slip condition is imposed on both the channel walls to avoid the development of boundary layers on them. The walls serve as an acoustical reflector, in addition to a flow blockage. The entire domain is decomposed into 7 numerical blocks. The surface of the airfoil is discretized by 600 cells; more than 70% of the cells are clustered on the suction side to resolve the vortical motions that may develop on the boundary layer. Total number of numerical cells is 1.7×10^5 . Present grid resolution is determined by reference to the two-dimensional convergence study of [5]. Numerical grid is shown in Fig. 1. The Reynolds number based on the chord length L and inflow mean velocity U_∞ , is 10,000. Inflow Mach number is altered from 0.1 to 0.4 to examine the dependence of wall resonant modes.

In the reference experiment [8], resonant tones were observed in the range $3^\circ \leq \alpha \leq 7^\circ$ with one degree increments for α at $M = 0.2$. Whereas no tones were detected on the pressure transducers at less than $\alpha = 3^\circ$, presumably due to the non-negligible level of background noise in the MWT, rather broadband spectra were observed at $\alpha > 7^\circ$. In the present numerical study, we focus on the tonal noise specifically between $\alpha = 3^\circ$ and 7° . In the parametric study on M and α , mostly two-dimensional calculations are performed. However, by increasing α , three-dimensional motions should develop, which affects aerodynamic force estimation. In the

NACA0012 case at the present Reynolds number, lift force is overpredicted in two-dimensional calculations at $\alpha \geq 7^\circ$ [3]. Therefore, we conduct three-dimensional calculations for the cases at $\alpha = 7^\circ$. In the present wind-tunnel configuration, two Mach numbers are compared: $M = 0.2$ and 0.3 in three dimensions. Spanwise length L is discretized with 128 cells, which leads to 2.2×10^7 numerical cells in total in three dimensions. On the spanwise grid convergence, we also conducted the case of doubled resolution, 256 cells for the spanwise domain length L , at $M = 0.2$ and $\alpha = 7^\circ$. Only minimal difference was observed in resonant frequency and statistics. We adopt the case of 128 grid cells for data presentation and discussion. For comparison, we reference our previous numerical study [3]. The NACA0012 airfoil was placed in a free stream at $M = 0.2$ and $Re = 10,000$, solved by an equivalent numerical approach. Three-dimensional results are also available for $\alpha = 7^\circ$ and 8° as the free-stream case.

4 Frequency Selection in a Wind Tunnel

4.1 Discrete Resonant Mode

Runyan and Watkins [12] derived the discrete modes of resonant frequency f , induced by a line dipole located in the middle of a hard-walled two-dimensional channel:

$$f = \frac{c_\infty \sqrt{1 - M^2}}{H} \left(m - \frac{1}{2} \right) \quad (1)$$

where c_∞ is speed of sound, $M = U_\infty/c_\infty$, H is channel height, and m is positive integer. Eq. (1) can be considered as the resonant relation of airfoil tones in a wind tunnel.

Firstly, the frequency dependence is examined on the angle of attack and Mach number. When an airfoil is placed in a uniform flow, Karman vortex shedding is induced by wake instability at small α . Then, as α increases, an acoustic feedback loop mechanism may arise, which significantly alters frequency. Fig. 2 compares the vortex shedding frequency of the present numerical cases, and the tone frequency observed in the MWT experiment. At $\alpha < 3^\circ$, two numerical cases agree fairly well, while no tones were

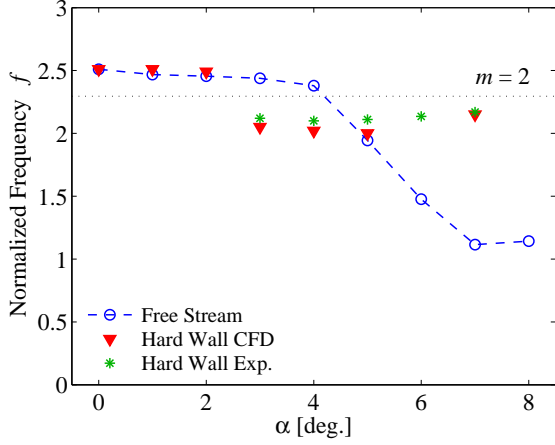


Fig. 2 Primary peak frequencies of v -velocity sampled at $0.1L$ downstream from the trailing edge for the inflow Mach number $M = 0.2$ and various angles of attack α , compared with the results of free-stream simulations [3] and an MWT experiment [8].

obtained in the experiment. However, at $\alpha = 3^\circ$, the shedding frequency of the hard-walled channel case discontinuously reduces nearly to that observed in the experiment. For $\alpha \geq 3^\circ$, the tone frequency of the present numerical results is almost fixed as observed in the experiment, except the two-dimensional case at $\alpha = 6^\circ$ where no tones can be recognized. On the other hand, the frequency of the free-stream case keeps decreasing up to $\alpha = 7^\circ$. At the angle of attack, the free-stream shedding frequency results in a considerable difference from the resonant tone of Eq. (1).

The same discrete nature can be observed at different Mach numbers. In the case $M = 0.1$, the normalized shedding frequencies are fixed relatively low around 1.5 at $\alpha \geq 3^\circ$, which approximately corresponds to the mode $m = 1$; the data are not shown. At $M = 0.3$ and 0.4 , the present results agree very well with those observed in the experiment, as shown in Fig. 3, with a few exceptions. In Fig. 3-(a), the tone frequency of the numerical result drops to the mode of $m = 1$ at $\alpha = 7^\circ$, which is inconsistent with the experimental observation. Indeed, this lower mode does occur in the experiment at $\alpha \geq 8^\circ$. Also in Fig. 3-(b), the secondary mode at $\alpha = 5^\circ$ in the numer-

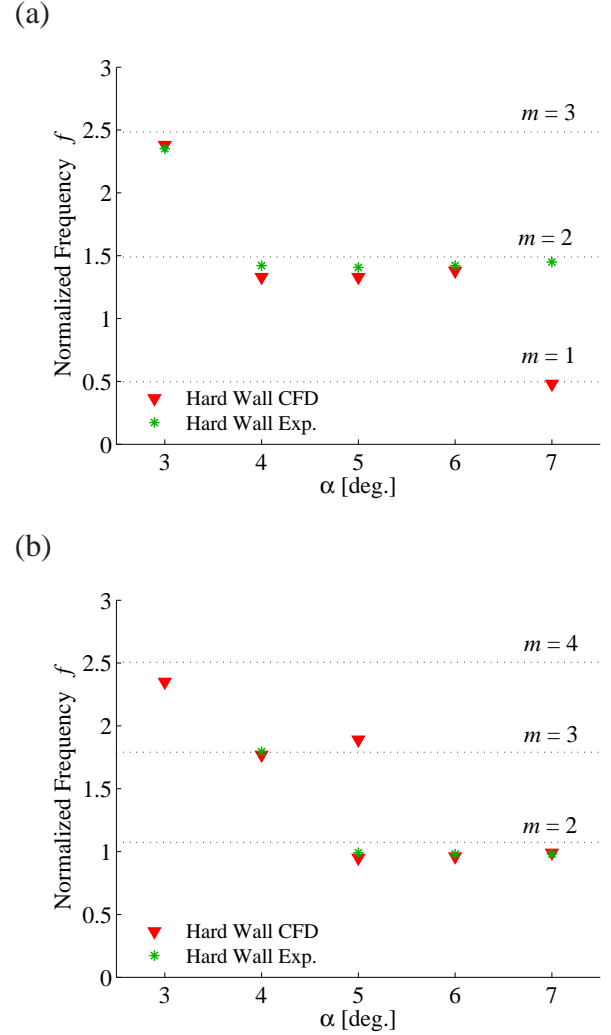


Fig. 3 Primary peak frequencies in the wake: (a) $M = 0.3$; (b) $M = 0.4$. In (b) at $\alpha = 5^\circ$, both primary and its sub-harmonic (or secondary) frequencies are plotted; at $\alpha = 7^\circ$, a two-dimensional result is shown for $M = 0.4$. Also see the caption of Fig. 2.

ical result matches the primary frequency in the experiment. The secondary mode in the numerical result is the sub-harmonic of the primary-mode frequency, which is very close to the shedding frequency of the free-stream case. Sampled in the wake, the primary mode is supposedly more amplified by the wake instability.

The difference in the frequency selection mechanism can be recognized in the vortex shedding patterns. Fig. 4 compares the three numerical cases at $\alpha = 5^\circ$. In the free-stream case Fig. 4-(a), the shedding frequency is determined primarily by the wake instability, still with a small effect of the feedback mechanism. A regular Karman vortex street forms in the wake, with only recognizable excitation of an instability wave near the trailing edge. On the other hand, other two wind-tunnel cases are apparently affected by the feedback mechanism associated with the resonant mode. Vortical motions arise in the suction-side boundary layer in the middle of the chord, unlike the free-stream case. Vortex shedding patterns seem affected by the superposed modes of discrete resonance, other than the primary mode.

The noise scattering from the airfoil confined in the walled passage seems rather different from common dipole sound emission [e.g., 4], due to the interference of wall reflection. Fig. 5 presents instantaneous sound pressure distributions that correspond to the primary resonant mode $m = 1$ to 4. As can be seen from the figures, pressure fluctuation is antisymmetric on the middle of the channel, $y = 0$. The integer m is determined by the number of wavelengths that exist in the wall normal directions above and below the airfoil. Due to the Doppler effect, acoustic waves traveling in the upstream direction have large amplitude with a lattice pattern formed by the interference, while the acoustic fluctuation in the wake region is rather small.

While the two-dimensional pressure fields show relatively clear lattice patterns, assuming a complete coherence in the spanwise direction, the resonant mode of three-dimensional calculations becomes somewhat obscure at a higher angle of attack. Still, the sampled spectra indicate that three-dimensional fields should also be under the influence of wall resonance, with

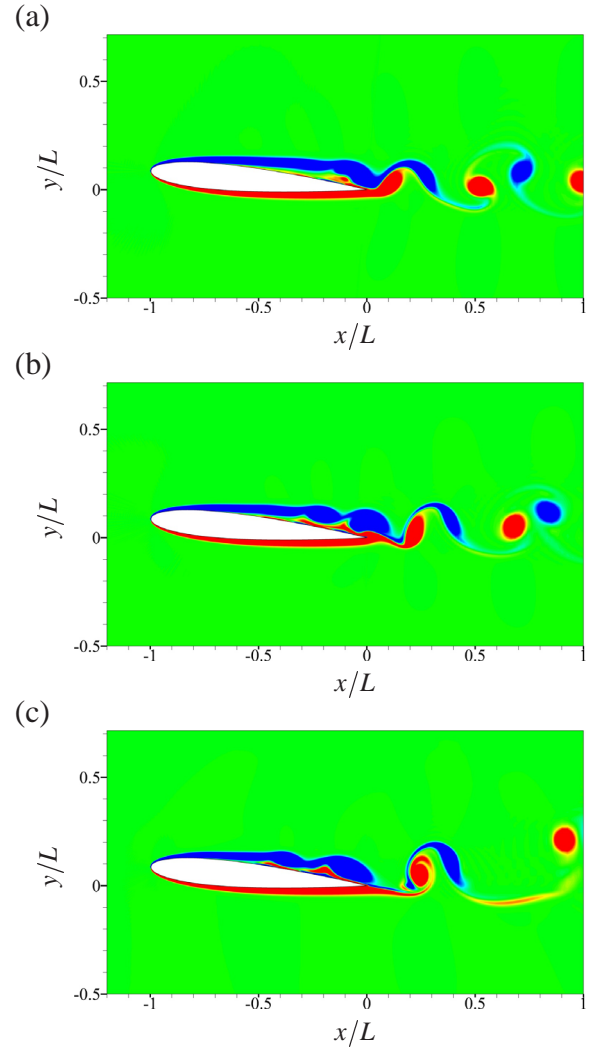


Fig. 4 Instantaneous ω_z vorticity distributions at $\alpha = 5^\circ$: (a) free stream case at $M = 0.2$; (b) wind tunnel case at $M = 0.2$; (c) wind tunnel case at $M = 0.3$. Color scale ranges between $-10 \leq \omega_z L/U_\infty \leq +10$ from blue to red.

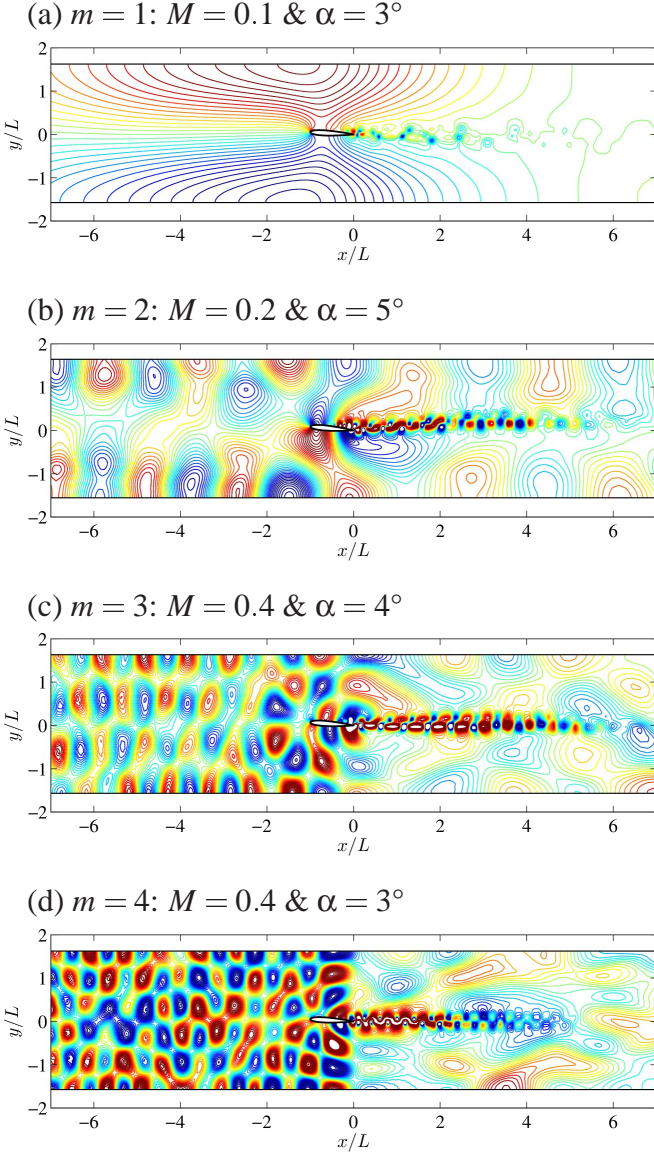


Fig. 5 Instantaneous pressure fluctuations for various primary antisymmetric resonant mode m of two-dimensional results. One contour level of pressure normalized by $\rho_\infty U_\infty^2$ denotes: (a) 1×10^{-2} ; (b) 3×10^{-3} ; (c) 2×10^{-3} ; (d) 1×10^{-3} . Total number of contour lines is 50.

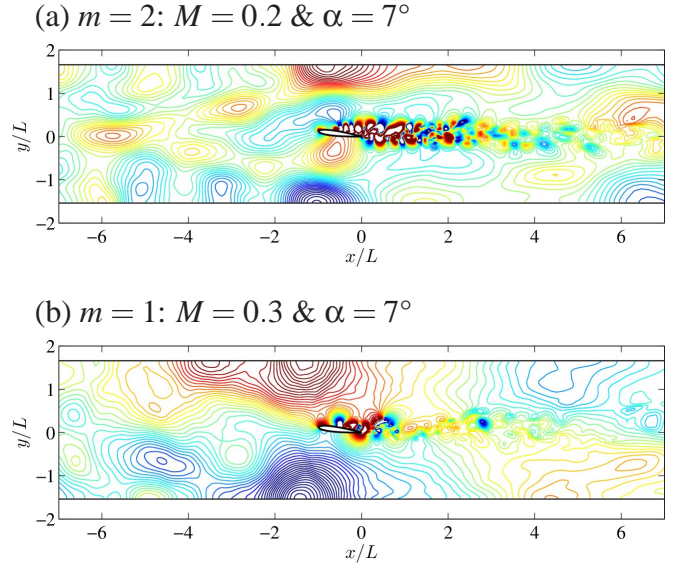


Fig. 6 Instantaneous pressure fluctuations of three-dimensional results on an x - y plane. One contour level denotes: (a) 8×10^{-4} ; (b) 4×10^{-3} . Also see the caption of Fig. 5.

tonal modes shown in Figs. 2 and 3 at $\alpha = 7^\circ$. Fig. 6 presents instantaneous x - y views of three-dimensional cases. Although the instantaneous views are affected by a broadband feature in the present cases, antisymmetric modes could be barely identified in the vertical direction across the airfoil.

4.2 Symmetric Resonant Mode

In addition to the resonance anti-symmetric on the middle of the test section, symmetric modes arise in the numerical simulation. The presence of a symmetric mode may contradict the dipole sound generation due to Karman vortex shedding. However, it is observed clearly at a low angle of attack, when an apparent anti-symmetric resonant mode does not occur. The discrete symmetric mode can be written as:

$$f = \frac{c_\infty \sqrt{1 - M^2}}{H} n \quad (2)$$

where n is positive integer.

Fig. 7 is an example of sound pressure distributions at $\alpha = 2^\circ$. The acoustic pressure fluctuation is nearly symmetric on $y = 0$. As in Fig. 2, the shedding frequency at this angle of attack coincides with that of the free stream case.

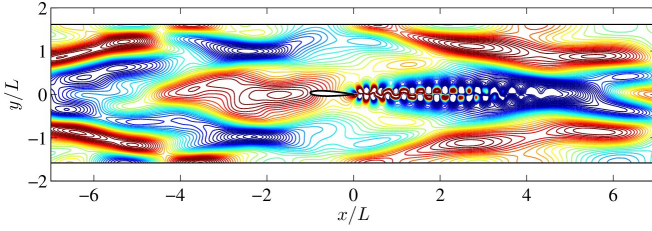


Fig. 7 An example of symmetric resonant modes: instantaneous pressure fluctuations at $\alpha = 2^\circ$ and $M = 0.2$. One contour level denotes 3×10^{-4} . Also see the caption of Fig. 5.

Therefore, the wall resonance of this symmetric mode does not seem to have direct relevance to the vortex shedding, assumingly independent of a feedback mechanism. When velocity fluctuations are sampled in the wake just behind the trailing edge, the frequency of vortex shedding $f = 2.5$ is an only distinguishable peak. Any symmetric modes are almost unrecognizable. However, when sampled in the acoustic region apart from the wake, symmetric modes present dominant peaks as shown in Fig. 8. As expressed in Eq. (2), these modes are composed of the basic tone $f = 1.53$ at $n = 1$, and its higher harmonics. On the other hand, a significant peak can be seen at the antisymmetric mode $m = 1$ in Eq. (1): $f = 0.766$. This corresponds to the subharmonic of the basic tone of symmetric modes. Therefore, we may assume that the presence of this lowest antisymmetric mode, relevant to antisymmetric vortex shedding, could activate its higher harmonic modes as symmetric resonance.

In Fig. 8, the vortex shedding frequency $f = 2.5$ also shows a sharp peak, but its spectral level is relatively small. We should also notice that there is another sharp peak at $f = 2.1$, which coincides with the resonant frequency at $\alpha \geq 3^\circ$, but not exactly with the mode $m = 2$ in Eq. (1): $f = 2.3$. Supposedly, this resonant frequency $f = 2.1$ is not solely determined by the resonance relation of Eq. (1), compared with other tones that agree very precisely with the predicted modes as in Fig. 8. Rather, it is selected via an acoustic feedback process where the instability of a suction-side boundary layer has a dominant effect. An acoustic feedback loop also deter-

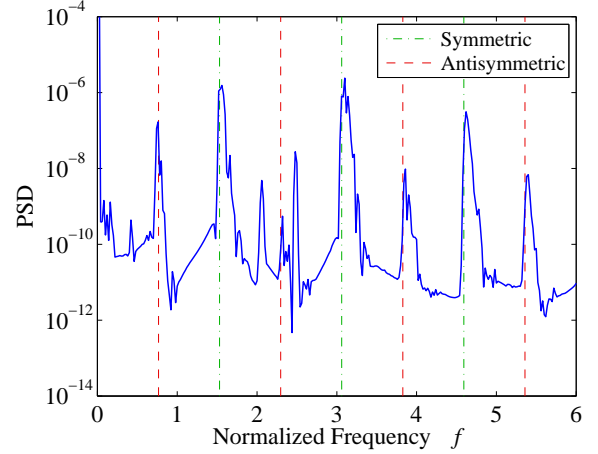


Fig. 8 Power spectral density of v -velocity sampled at $0.5L$ above the trailing edge at $\alpha = 2^\circ$ and $M = 0.2$.

mines discrete resonant modes [2]. Unstable, sufficiently amplified frequencies close to the wall resonant mode would be selected in the feedback mechanism.

5 Aerodynamics under the Influence of Wall Resonance

It is of great interest how the acoustic resonance may affect the aerodynamic measurements of a low Reynolds number flow in the closed test section. In the numerical study [5], it was shown that the onset of an acoustic resonance could improve aerodynamic performance by forming a laminar separation bubble behind the leading edge at $Re = 10,000$. The formation of a separation bubble at the forward part of an airfoil develops a transitional boundary layer that prevents bulk separation, initiated by the acoustic disturbances fed back at the leading edge.

In the present study, lift forces of NACA0012 are compared among the numerical results of the free-stream case, and the hard-walled wind-tunnel cases at $M = 0.2$ and 0.3 , in addition to a wind-tunnel experiment conducted at fairly low Mach number in a common laboratory environment [9], as shown in Fig. 9. In the free-stream simulations, three-dimensionality becomes significant at $\alpha \gtrsim 7^\circ$, where two-dimensional calculations overestimate lift. Here, three-dimensional

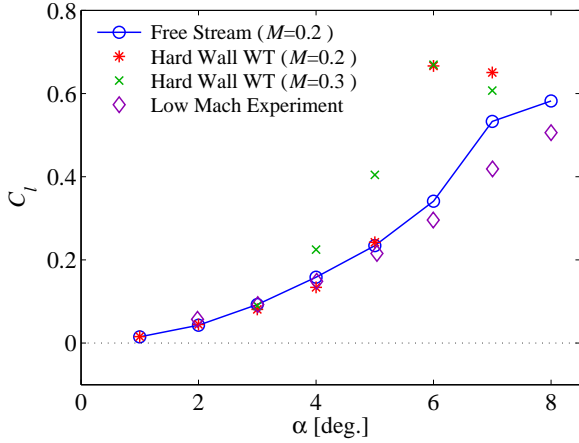


Fig. 9 The comparison of time-averaged lift coefficients between three numerical cases and an experimental result of a low Mach case [9].

results are presented both for $\alpha = 7^\circ$ and 8° . The free-stream calculations agree well with the low Mach experiment at $\alpha \leq 6^\circ$. However, in spite of the three-dimensionality considered in the simulations, appreciable differences exist at $\alpha \geq 7^\circ$. Moreover, the lift in the wind-tunnel computation becomes even higher than that of the free-stream case, in a considerable range of angle of attack, also depending on Mach number. This can be regarded as the modification of hydrodynamic states via strong acoustic resonance.

In the referenced experiment [9], the airfoil of chord length 75 [mm] was used to attain $Re = 10,000$ in a ground environment. Thus, the flow Mach number is estimated to be $M \simeq 0.006$. Since the acoustic component of velocity fluctuation has the Mach number dependence of $M^{3/2}$ in two-dimensional acoustic scattering, the magnitude of velocity disturbance fed back into the boundary layer would be about 0.5% of the present numerical cases at $M = 0.2$. The difference should have a great effect on the development of hydrodynamic unsteadiness in the suction-side boundary layer. Similarly, in the present numerical cases, a higher Mach number flow often results in strong acoustic resonance, as observed in the difference of $M = 0.2$ and 0.3 in Fig. 9.

The difference in aerodynamic characteristics is investigated in more details. Pressure distribu-

tions on the suction side are compared in Fig. 10, among the free-stream case, the wind-tunnel simulation, and the MWT experiment at $M = 0.2$, for $\alpha = 3^\circ, 5^\circ$, and 7° . As the resultant lift forces agree at $\alpha = 3^\circ$ & 5° , the two numerical cases show almost no discernible difference, regardless of the flow-passage walls. Besides, they also coincide well with the experimental profiles obtained through the graphical image of pressure-sensitive paint [8]. However, at $\alpha = 7^\circ$, an appreciable deviation arises in the pressure distribution, while all the cases present a plateau, or flat profile behind steep adverse pressure gradient at the leading edge, and a following pressure recovery region toward the trailing edge. The plateau often denotes the presence of an adjacent separation bubble. As the separated flow reattaches in the middle of the chord, a relatively steep pressure recovery would occur behind the reattachment. This resembles the “separation ramp” concept [6], which is considered to be a favorable feature for better aerodynamic performance. In Fig. 10, the profile of the wind-tunnel simulation indicates a less pressure recovery at the leading-edge separation, and an earlier occurrence of a separation ramp, compared with the free-stream case. However, the experimental result is somewhat between these two numerical results: the pressure recovery at the leading-edge separation agrees with the free-stream case, while the separation ramp at the trailing edge better coincides with the wind-tunnel computation.

In Fig. 11, the separation bubbles are drawn on the time-averaged velocity field of the three numerical cases that were compared in the lift curve diagram Fig. 9: the free-stream case at $M = 0.2$, and the hard-wall wind-tunnel computations at $M = 0.2$ and 0.3. At $\alpha = 5^\circ$, the free-stream and wind-tunnel cases almost perfectly match at $M = 0.2$, similarly to the pressure distributions Fig. 10. They exhibit a typical separation bubble of a trailing-edge stall, elongated in the streamwise direction. However, the wind-tunnel case at $M = 0.3$ reduces the size of a separation bubble, although the separation location is almost identical with the other two cases. Usually, a trailing-edge stall causes a fairly flat pressure profile toward the trailing edge. The aero-

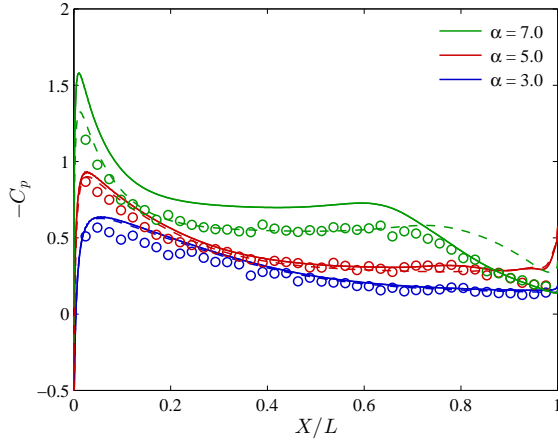


Fig. 10 Time-averaged pressure distributions on the suction side of the airfoil at $M = 0.2$: —, wind-tunnel case; - - -, free-stream case; \circ , MWT experiment.

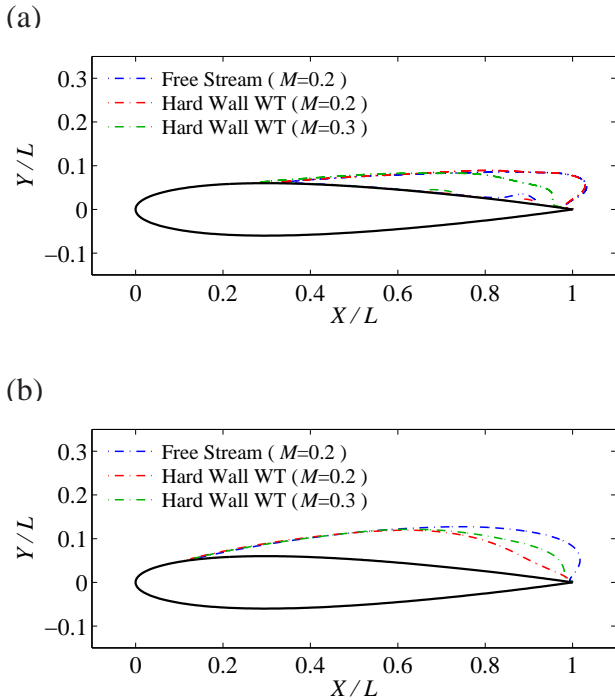


Fig. 11 The comparison of separation bubbles of time-averaged velocity fields between the free stream case, and the hard-wall wind tunnel cases at $M = 0.2$ and 0.3 at: (a) $\alpha = 5^\circ$; (b) $\alpha = 7^\circ$.

dynamic performance is lowered if the separation location shifts to the leading edge at a higher angle of attack, without any reattachment in the middle of the chord [5]. The acoustic resonance enforces the suction-side vortical motions, shortening the trailing-edge separation bubble, as also understood from Fig. 4.

On the other hand, as shown in Fig. 11-(b) at $\alpha = 7^\circ$, the size of separation bubbles varies among these three-dimensional cases. While the separation locations coincide well just downstream of 10% chord, the acoustic resonance apparently affects the mixing strength of the separation shear layer. Still, none of the present cases causes reattachment upstream of the trailing edge. The wind-tunnel case at $M = 0.2$ exhibits the smallest separation bubble, while the higher Mach number case $M = 0.3$ settles in the middle, unlike the cases at $\alpha = 5^\circ$ shown in Fig. 11-(a). Although not shown in Fig. 10, the upper-surface pressure profiles of the hard-walled wind-tunnel cases are very similar between $M = 0.2$ and 0.3 , in spite of a recognizable difference in separation bubbles. Presumably, this difference is caused by the stability of the shear layer that depends on a base-flow Mach number. As will be shown below, the suction-side boundary layer exhibits significant three-dimensional motions, developed in adverse pressure gradient. Nonetheless, we should note that the separation ramp behavior, observed in Fig. 10, is not necessarily the evidence of reattachment in the middle of the chord, unlike the numerical study of thinner cambered airfoils [5].

Finally, the three-dimensional motions are examined via visualization at $\alpha = 7^\circ$. Fig. 12 shows the vortex visualization of the Q -criterion colored with streamwise vorticity; nominally two-dimensional spanwise vortical motions can be recognized by green. Behind the leading edge, the separation shear layer is first recognized, elongated in the streamwise direction, especially in the free-stream case. Then, it develops into two-dimensional instability waves. However, right after the spanwise vortices roll up, they are broken up into small longitudinal eddies, showing a transitional boundary layer, still sustaining large spanwise motions. In the present

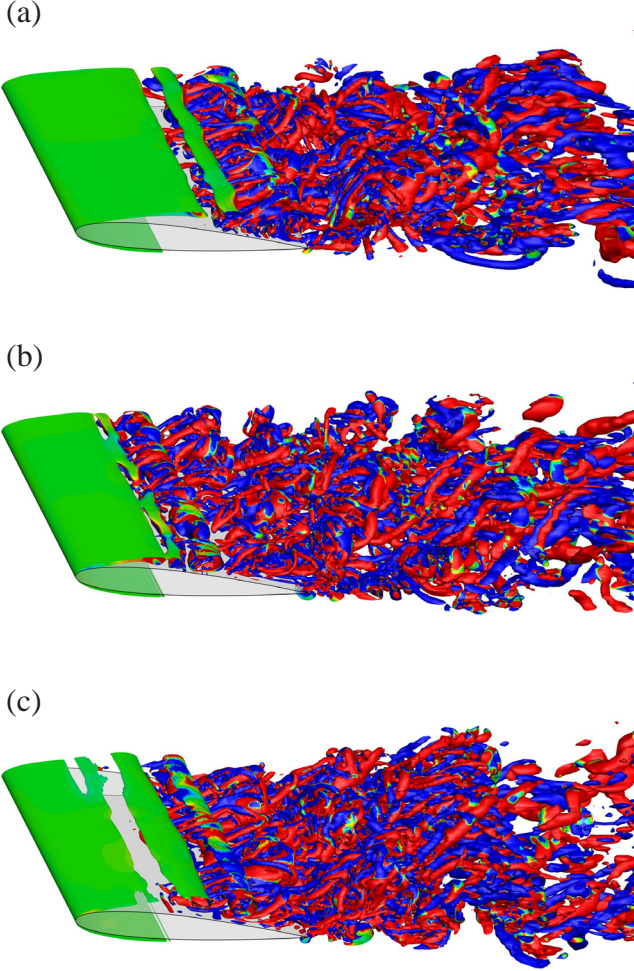


Fig. 12 The comparison of three-dimensional numerical results at $\alpha = 7^\circ$, via instantaneous Q -vortex isosurfaces at $Q = 10(U_\infty/L)^2$, colored by streamwise vorticity $\omega_x L/U_\infty$ ranging between -1 and $+1$ from blue to red: (a) free stream case at $M = 0.2$; (b) wind tunnel case at $M = 0.2$; (c) wind tunnel case at $M = 0.3$.

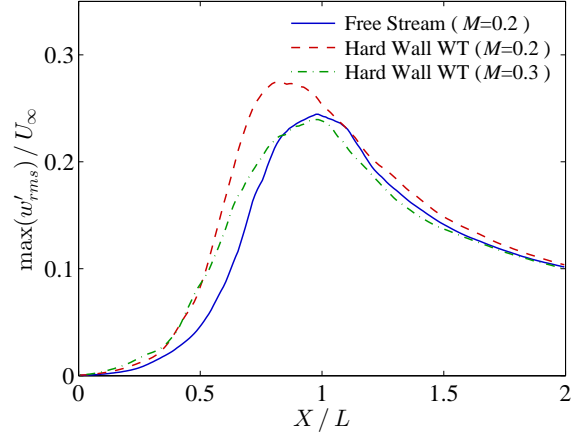


Fig. 13 The rms fluctuation of w -velocity of three-dimensional cases at $\alpha = 7^\circ$, above the airfoil ($0 \leq X/L \leq 1$) and in the wake ($1 < X/L$). Local maxima at each X location is shown.

results, the wind-tunnel case at $M = 0.2$ seems to present the most upstream transition of vortical motions, as in Fig. 12-(b). In spite of stronger acoustic resonance, the higher Mach number case slightly delays the transition at $M = 0.3$ shown in Fig. 12-(c). The free-stream case sustains a relatively large laminar region behind the leading edge as in Fig. 12-(a), but also supposedly affected by the acoustic feedback effect associated with a trailing-edge noise, when compared with the extremely lower Mach-number case in Fig. 9, conducted in a common laboratory environment [9].

Spanwise velocity fluctuation is indicative of the extent of transitional boundary layer development. Fig. 13 compares the chordwise growth of rms spanwise velocity obtained in the three-dimensional results at $\alpha = 7^\circ$. While the free-stream case shows the least w fluctuation down to 80% chord, both the wind-tunnel cases present apparently larger growth rates at the forward part of the chord, due to the acoustic resonance. The hard-wall wind tunnel case at $M = 0.2$ attains the largest rms value, about 12% larger than the free-stream case. However, the maximum value of the hard-wall case at $M = 0.3$ is just comparable with the free stream case. This is presumably the stabilization effect of a higher Mach number flow. The instability of a shear layer would be low-

ered by increasing Mach number. Still, the acoustic disturbance is large enough to reduce the size of the separation bubble comparing to the free-stream case, by stimulating transitional motions in the suction-side boundary layer.

6 Conclusions

The wind-tunnel wall resonance was investigated numerically, associated with airfoil tones of dipole nature at $Re = 10,000$. Confined in a hard-walled passage, two-dimensional airfoil flows solved on a compressible Navier-Stokes code successfully reproduced discrete tones that approximately satisfies the resonant modes suggested by Runyan and Watkins [12], clearly affected by the wall resonance, compared to the free-stream case. However, the discontinuous change of tonal modes on angles of attack indicates that the tonal frequency would be determined via the instability of suction-side boundary layer and the acoustic feedback mechanism, as originally suggested by [2], not solely the geometrical relation of resonance [12]. The present results agree very well with the tonal modes observed in our previous experimental study [8].

The onset of wall-resonant modes affects not only the observed aerodynamic sound, but also the aerodynamic characteristics as time-averaged quantities. In the present case, external wall resonance amplifies the hydrodynamic instability waves that may develop into significant vortical motions in the suction-side boundary layer. The transitional boundary layer driven by the resonance reduces the size of separation bubbles, which eventually increases the lift. At relatively higher angle of attack, $\alpha = 7^\circ$, transitional behavior is already observed in the free-stream result, with spanwise vortices breaking-up into longitudinal eddies. However, the wind-tunnel calculation accelerates the transition, diminishing the laminar region behind the leading edge. The reduced size of the separation bubble also significantly alters the surface pressure profile with a separation ramp, as if the aerodynamic performance of an airfoil were improved.

7 Contact Author Email Address

The corresponding author can be contacted at ikedat@chofu.jaxa.jp (Tomoaki Ikeda).

References

- [1] M. Anyoji, K. Nose, S. Ida, D. Numata, H. Nagai, and K. Asai. Aerodynamic measurements in the Mars Wind Tunnel at Tohoku University. *AIAA Paper 2011-0852*, 2011.
- [2] H. Arbey and J. Bataille. Noise generated by airfoil profiles placed in a uniform laminar flow. *J. Fluid Mech.*, 134:33–47, 1983.
- [3] T. Ikeda and T. Atobe. Numerical studies of acoustic effects on 2D airfoil aerodynamics at a low Reynolds number. *AIAA Paper 2012-0700*, 2012.
- [4] T. Ikeda, T. Atobe, and S. Takagi. Direct simulations of trailing-edge noise generation from two-dimensional airfoils at low Reynolds numbers. *J. Sound Vib.*, 331(3): 556–574, 2012.
- [5] T. Ikeda, D. Fujimoto, A. Inasawa, and M. Asai. Unsteady aerodynamic characteristics of cambered four-digit NACA airfoils at low Reynolds number. *AIAA Paper 2014-0049*, 2014.
- [6] M. D. Maughmer and D. M. Somers. Design and experimental results for a high-altitude, long-endurance airfoil. *J. Aircraft*, 26(2):148–153, 1989.
- [7] E. C. Nash, M. V. Lowson, and A. McAlpine. Boundary-layer instability noise on aerofoils. *J. Fluid Mech.*, 382:27–61, 1999.
- [8] K. Nose, N. Sakai, D. Numata, H. Nagai, K. Asai, T. Ikeda, and T. Atobe. Unsteady aerodynamic experiment of NACA0012 airfoil at low Reynolds number. In *Proc. Eighth Int. Conf. Flow Dynamics*, pages 244–245, Sendai, Japan, 2011.

- [9] T. Ohtake, Y. Nakae, and Y. Motohashi. Nonlinearity of the aerodynamic characteristics of NACA0012 aerofoil at low Reynolds numbers. *J. Japan Soc. Aeron. Space Sci.*, 55(644):29–35, 2007.
- [10] R. Parker. Resonance effects in wake shedding from parallel plates: calculation of resonant frequencies. *J. Sound Vib.*, 5(2):330–343, 1967.
- [11] R. W. Paterson, P. G. Vogt, M. R. Fink, and C. L. Munch. Vortex noise of isolated airfoils. *J. Aircraft*, 10(5):296–302, 1973.
- [12] H. L. Runyan and C. E. Watkins. Considerations on the effect of wind-tunnel walls on oscillating air forces for two-dimensional subsonic compressible flow. Technical Note 2552, NACA Langley Aeronautical Laboratory, Langley Field, VA, 1951.
- [13] S. Takagi and Y. Konishi. Frequency selection mechanism of airfoil trailing-edge noise. *J. Aircraft*, 47(4):1111–1116, 2010.

Acknowledgements

This work was supported by Grant-in-Aid for Scientific Research (C) from Japan Society for the Promotion of Science (Grant No. 25420139). Computational resources were provided by JAXA Supercomputer System.

Copyright Statement

The authors confirm that they, and/or their company or organization, hold copyright on all of the original material included in this paper. The authors also confirm that they have obtained permission, from the copyright holder of any third party material included in this paper, to publish it as part of their paper. The authors confirm that they give permission, or have obtained permission from the copyright holder of this paper, for the publication and distribution of this paper as part of the ICAS 2014 proceedings or as individual off-prints from the proceedings.